

On the magnetic field in M51 ULX-8

M. J. Middleton¹, M. Brightman², F. Pintore³, M. Bachetti⁴, A. C. Fabian⁵,
F. Fürst⁶ & D. J. Walton⁵

1. Department of Physics and Astronomy, University of Southampton, Highfield, Southampton SO17 1BJ, UK

2. Cahill Center for Astrophysics, California Institute of Technology, 1216 East California Boulevard, Pasadena, CA 91125, USA

3. INAF - IASF Milano, Via E. Bassini 15, I-20133 Milano, Italy

4. INAF-Osservatorio Astronomico di Cagliari, via della Scienza 5, I-09047 Selargius, Italy

5. Institute of Astronomy, University of Cambridge, Madingley Road, Cambridge CB3 0HA, UK

6. European Space Astronomy Centre (ESAC), Science Operations Departement, 28692 Villanueva de la Canada, Madrid, Spain

13 March 2019

ABSTRACT

The reported discovery of a cyclotron resonance scattering feature (CRSF) in the spectrum of M51 ULX-8 may provide an important clue as to the nature of the magnetic field in those ultraluminous X-ray sources hosting neutron stars. In this paper we present the covariance (linearly correlated variability) spectrum of M51 ULX-8 on long (> 2000 s) timescales. This allows us to unambiguously decompose the spectrum which requires multiple components in order to explain the broad-band emission. Having a clearer picture of the spectral decomposition leads to various tests for the dipole field strength of the neutron star which can be extended to other ULXs when certain criteria are met. In the case of M51 ULX-8, we rule out a very strong ($\sim 10^{15}$ G) dipole solution with either a sub- or super-critical disc. Instead, our tests indicate an upper limit on the dipole field of $\sim 10^{12}$ G and a classical super-critical inflow, similar to that inferred in other ULXs found to harbour neutron stars, although we do not rule out the presence of an additional, strong ($\sim 10^{15}$ G) multipole field falling off steeply with distance from the neutron star.

Key words: accretion, accretion discs – X-rays: binaries, black hole, neutron star

1 INTRODUCTION

The discovery of ultraluminous pulsars (ULPs or PULXs, Bachetti et al. 2014; Fürst et al. 2016; Israel et al. 2017a, b; Carpano et al. 2018) has revolutionised the field of ultraluminous X-ray sources (ULXs, see the review of Kaaret et al. 2017). Whilst ULXs were long considered to be possible candidates for hosting intermediate mass black holes (IMBHs), it was immediately apparent that the explanation for the extreme observed luminosities ($> 10^{39}$ erg s⁻¹) in at least *some* ULXs was accretion in excess of the classical Eddington limit onto common-place primary objects — in this case neutron stars. However, whilst the mass-regime of the compact object in ULXs has been at least partly resolved (we note that candidate IMBHs still remain, e.g. Farrell et al. 2009), the relative number of black hole to neutron star primaries in ULXs (see King, Lasota, & Kluzniak 2017; Middleton & King 2017) and the nature of the accretion flow in ULPs remain outstanding puzzles. At the centre of the debate is the strength of the surface dipole field and any multipolar component. Should the dipole field strength be similar to that of Galactic HMXBs ($\sim 10^{12}$ G — e.g. Fürst et al. 2014; Tendulkar et al. 2014; Yamamoto et al. 2014; Bellm et al. 2014) then it is quite plausible that the flow will be super-critical

($\dot{m}/\dot{m}_{\text{Edd}} > 1$ where \dot{m}_{Edd} is the Eddington accretion rate) at radii greater than the magnetospheric truncation radius (r_{M}). In this case, the super-critical portion of the disc will have a large — close to unity — vertical scale-height and winds will be launched from the surface (see Shakura & Sunyaev 1973; Poutanen et al. 2007 and the simulations of Ohsuga et al 2009; Sadowski et al. 2014; Jiang, Stone & Davis 2014). Within r_{M} , the flow will take the form of an accretion curtain (Mushtukov et al. 2017; 2019) and shock-heated column as material falls onto the magnetic poles. Due to collimation by the disc and outflows beyond r_{M} , it is expected that the intrinsic luminosity is then partially geometrically beamed (see King 2009). Conversely, should the dipole field strength be very high (typically $> 10^{13}$ G) then it is quite probable that the disc will truncate before becoming locally super-critical. The geometry in this case is then expected to take the form of a geometrically thin disc down to r_{M} , an accretion curtain and shock-heated column. Rather than a super-critical disc and geometrical beaming, super-Eddington luminosities can then be explained by a magnetic pressure supported accretion column (Basko & Sunyaev 1976) and high field strength, the latter allowing for a substantially increased luminosity from a reduction in the electron scattering cross-section

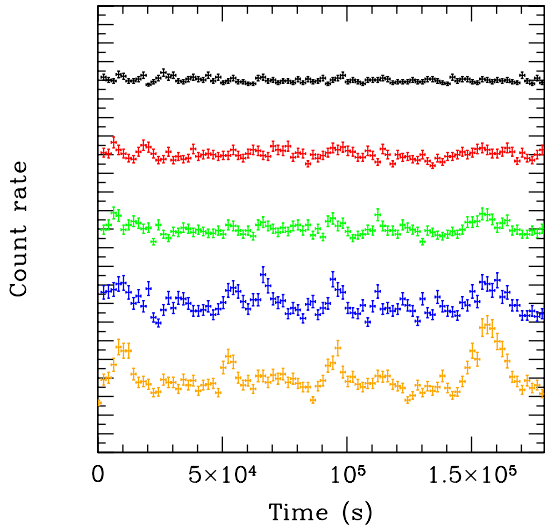


Figure 1. Background-subtracted *Chandra* lightcurves of M51 ULX-8 rebinned to 2000s. The energy bands from top to bottom are 0.5–0.7 keV (black), 0.7–1 keV (red), 1–1.3 keV (green), 1.3–2 keV (blue) and 2–8 keV (orange). The lightcurves are offset in count rate for clarity but are on the same absolute scale with small and large ticks indicating 0.005 counts s^{-1} and 0.01 counts s^{-1} respectively. The appearance of long timescale variability at high energies is apparent and may resemble the super-orbital quasi-periodicities seen in other ULPs (but on much shorter timescales in this case).

(e.g. Herold 1979; Paczynski 1992; Thompson & Duncan 1995; Mushtukov et al. 2015)

Certainly there are compelling reasons to believe either scenario described above: the measured rate of spin-up for those ULPs found thus far would seem to imply dipole field strengths $\sim 10^{11} - 10^{13}$ G (e.g. King & Lasota 2016; Christodoulou et al. 2016; Fürst et al. 2016; King, Lasota & Kluzniak 2017; Carpano et al. 2018), whilst a higher-strength dipole scenario can more easily explain the sinusoidal profile of the pulsations (Mushtukov et al. 2017).

Reported in Liu & Mirabel (2005), M51 ULX-8 is one of the brightest ULXs associated with this interacting galaxy and can be excluded as a foreground source from its identified stellar counterpart (Terashima et al 2006) and as an AGN from the strong curvature in the X-ray spectrum. With the identification of a cyclotron resonance scattering feature (CRSF) in M51 ULX-8 (Brightman et al. 2018) we have been provided an opportunity to directly probe the nature of the magnetic field in the vicinity of what is assumed to be a neutron star. As Brightman et al. (2018) report, if the line at ≈ 4.5 keV, is identified as a proton-CRSF (pCRSF) it would imply either a high-strength ($\sim 10^{15}$ G) dipole field or a very strong, higher-order multipole field close to the neutron star surface (e.g. Israel et al. 2017b). Alternatively, should the feature be identified as an electron-CRSF (eCRSF) then the dipole (or multipole) field is expected to be far weaker at $\sim 10^{11}$ G (depending on how far from the neutron star surface the line is actually formed).

In this letter we present the time-resolved properties of M51 ULX-8 which allows us to rule out the presence of a high strength dipole field and identify the likely nature of the accretion flow.

2 DATA ANALYSIS

Following the procedures outlined in Brightman et al. (2018), we extract and analyse the same *Chandra* data of M51 ULX-8 in which the CRSF was discovered — OBSID: 13813 with an effective exposure of ≈ 180 ks. In Figure 1 we plot the energy-resolved, background-subtracted lightcurves (0.5–0.7, 0.7–1.0, 1–1.3, 1.3–2 and 2–8 keV) binned on 2000s which indicate that the vast majority of the variability is associated with energies > 2 keV. Although few in number, we note that the recurrent peaking behaviour at high energies is somewhat reminiscent of the longer timescale behaviour seen in ULPs (e.g. Walton et al. 2016b) but in this case, on far shorter timescales (\sim tens of hours rather than \sim tens of days in ULPs). Should this behaviour be periodic or quasi-periodic (we note that we have an insufficient number of peaks to confirm any such claim), the timescale would be enormous for the rotation period of the neutron star but *could* instead indicate precession of a super-critical accretion flow (e.g. Pasham & Strohmayer 2013; Middleton et al. 2018). Indeed, the variability does not resemble typical band-limited noise and the clear trend of the source being brighter when spectrally harder (i.e. during the peaks in the hard X-ray band) is a corollary of the latter model (e.g. Middleton et al. 2015).

We further break the 2–8 keV band into three narrower sub-bands (2–3, 3–4 and 4–8 keV) and obtain an estimate for the power in each and in the pre-existing 0.5–0.7, 0.7–1.0, 1–1.3 and 1.3–2 keV bands by fast-Fourier transforming each lightcurve, broken into 5 segments (with each segment containing 16×2000 s bins). The power in each band is given by $\langle |X_\nu|^2 \rangle = \langle X_\nu^* X_\nu \rangle$ where X_ν is the Fourier transform of the lightcurve segment, * indicates the complex conjugate and the angle brackets indicate the average over segments (we note that, as the number of segments in this case is only 5, the resulting errors will only be approximately Gaussian). We proceed to obtain the intrinsic (noise-subtracted) coherence (Vaughan & Nowak 1997) relative to the 1–1.3 keV band from the complex-valued cross spectrum: $C_\nu = X_\nu^* Y_\nu$, where X_ν and Y_ν are the Fourier transforms of the reference lightcurve (in this case the 1–1.3 keV lightcurve) and comparison lightcurve respectively at Fourier frequency, ν . The linearly correlated coherence (which measures how well one lightcurve can be mapped to another by a simple linear transformation) is then given by $|\langle C_\nu \rangle|^2 / (\langle |X_\nu|^2 \rangle \langle |Y_\nu|^2 \rangle)$ where all of the powers in the denominator have been corrected for Poisson noise (and the numerator is corrected following the recipe of Vaughan & Nowak 1997). From the product of the coherence and noise-subtracted power in the comparison band, we then obtain the covariance (see Wilkinson & Uttley 2009; Uttley et al. 2014) and integrate from 0.03125–0.25 mHz.

The covariance in absolute (rms) units is obtained for six out of the seven bins (it cannot be extracted for our lowest energy bin) and is loaded into XSPEC (Arnaud et al. 1996). This covariance spectrum is shown in Figure 2 along with the time-averaged data, both unfolded through the instrumental response, and a power-law of zero index and unity normalisation (such that the process of unfolding does not bias the appearance of the spectrum). The figure indicates that the variable component does not account for the entire 0.3–8 keV emission, requiring at least one separate component at softer energies.

To explore the nature of the source, we require a spectral decomposition which explicitly includes the component revealed by the covariance. We proceed to fit the covariance spectrum with a simple, absorbed, exponentially cut-off power-law (TBABS**CUTOFFPL*) with abundances from Wilms et al.

Table 1. Spectral fitting results

Covariance spectral fit (TBABS*GABS*CUTOFFPL)		Time-averaged spectral fit (fixed line) (TBABS*[DISKBB + GABS*CUTOFFPL])		Time-averaged spectral fit (free line) (TBABS*[DISKBB + GABS*CUTOFFPL])	
nH ($\times 10^{22} \text{cm}^{-2}$)	0.08 (fixed)	nH (10^{22}cm^{-2})	0.05 ± 0.02	nH (10^{22}cm^{-2})	$0.11^{+0.04}_{-0.03}$
		kT _{dbb} (keV)	0.58 ± 0.03	kT _{dbb} (keV)	$0.41^{+0.07}_{-0.08}$
		N _{dbb}	$0.12^{+0.03}_{-0.02}$	N _{dbb}	$0.46^{+0.76}_{-0.22}$
		L _{dbb} ($\times 10^{39} \text{erg s}^{-1}$)	$2.33^{+0.08}_{-0.07}$	L _{dbb} ($\times 10^{39} \text{erg s}^{-1}$)	$2.03^{+0.12}_{-0.14}$
Γ	$-0.75^{+1.10}_{-0.81}$	Γ	-0.75 (fixed)	Γ	-0.75 (fixed)
E _{cutoff} (keV)	$1.61^{+9.04}_{-0.40}$	E _{cutoff} (keV)	1.61 (fixed)	E _{cutoff} (keV)	1.61 (fixed)
N _{cutoff} ($\times 10^{-5}$)	$2.05^{+0.47}_{-0.77}$	N _{cutoff} ($\times 10^{-5}$)	$3.34^{+0.17}_{-0.18}$	N _{cutoff} ($\times 10^{-5}$)	$5.30^{+1.76}_{-0.85}$
		L _{cutoff} ($\times 10^{39} \text{erg s}^{-1}$)	$2.52^{+0.08}_{-0.09}$	L _{cutoff} ($\times 10^{39} \text{erg s}^{-1}$)	$4.00^{+0.31}_{-0.24}$
E _{cyc} (keV)	4.52 (fixed)	E _{cyc} (keV)	4.52 (fixed)	E _{cyc} (keV)	$4.72^{+0.17}_{-0.13}$
σ (keV)	0.11 (fixed)	σ (keV)	0.11 (fixed)	σ (keV)	$0.96^{+0.41}_{-0.26}$
N _{cyc}	< 263	N _{cyc}	$0.23^{+0.06}_{-0.05}$	N _{cyc}	$1.63^{+1.57}_{-0.67}$
$\chi^2/\text{d.o.f}$	1.16/2	$\chi^2/\text{d.o.f}$	244.48/216	$\chi^2/\text{d.o.f}$	239.56/214
null P value	0.56	null P value	0.09	null P value	0.11

Notes: Best-fitting model parameters for the fit to the covariance and time-averaged data of M51 ULX-8 (see Figure 2) including the unabsorbed 0.3-8 keV luminosity of each component. Formal errors are quoted at 1σ (see Section 2 for further discussion).

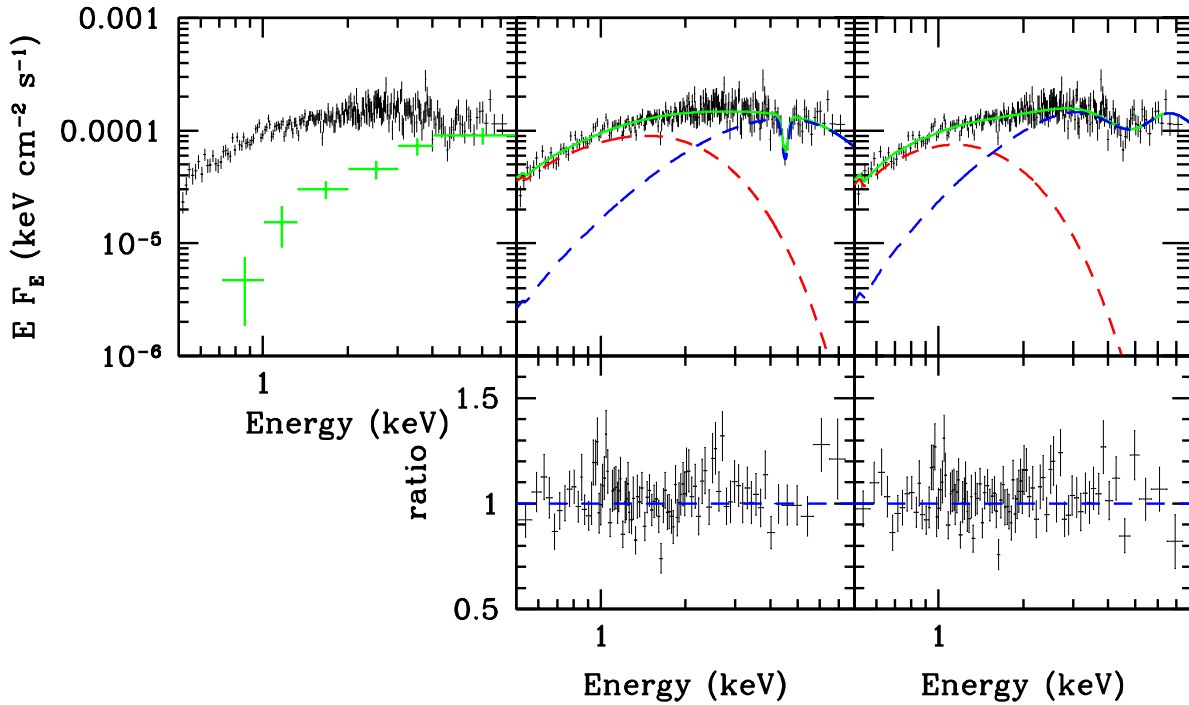


Figure 2. *Left:* the covariance (green) and time-averaged (black) spectral data unfolded through a power-law of zero index and unity normalisation (such that there is no bias from unfolding). *Centre and right:* The time-averaged data modelled and unfolded through TBABS*(DISKBB + GABS*CUTOFFPL) with the parameters of the CUTOFFPL fixed to the best-fitting values from modelling the covariance spectrum (with the exception of the normalisation) and line parameters fixed (centre panel) and free (right-hand panel) respectively. The DISKBB component is shown in dashed red, the CUTOFFPL component is shown in dashed blue and the combination (including absorption by the CRSF line) is shown in solid green. The lower panels show the residuals to the best-fitting model (data/model) re-binned for clarity in each case.

(2000) and column density set to that reported in Brightman et al. (2018). The cut-off power-law takes the form: $A(E) = KE^{-\Gamma} \exp(-E/E_{\text{cutoff}})$, where Γ is the power-law photon index, E_{cutoff} is the e-folding energy of the exponential roll-off and K is the normalisation. This model has previously been used to describe the high energy emission of ULXs (e.g. Bachetti et al. 2013; Pintore et al. 2017) and most recently emission from the accretion column in ULPs (e.g. Walton et al. 2018a, b). Although we do not have the spectral resolution to isolate the contribution (or lack thereof) by the CRSF to the covariance, we include an absorption line (described in XSPEC by a GABS component) with centroid energy (4.52 keV) and width (0.11 keV) set by fits to the time-averaged spectrum in Brightman et al. (2018) but with the line normalisation free to vary. A good statistical description of the data is obtained (see Table 1 for parameter values and formal 1σ errors) with parameter values (Γ and E_{cutoff}) for the cut-off power-law similar to those reported for the ULP, NGC 7793 P13 (Walton et al. 2018a).

We proceed to fit the time-averaged spectrum (background-subtracted and re-binned for chi-squared fitting: see Brightman et al. 2018) with a model composed of a CUTOFFPL component at high energies, a disc blackbody (DISKBB) at lower energies, and the CRSF (GABS) convolved with the CUTOFFPL component only. We fix the index (Γ) and cutoff energy (E_{cutoff}) to the best-fitting values from our fits to the covariance spectrum and allow the normalisation to be free to vary (but fixing the lower limit to the value returned from the fits to the covariance spectrum). We also allow the neutral column to be free to vary, setting the lower limit to the Galactic line-of-sight column density in the direction of M51, $2 \times 10^{20} \text{ cm}^{-2}$ (Dickey & Lockman 1990). We initially fix the CRSF parameters (line energy and width) to those in Brightman et al. (2018) and obtain a statistically acceptable fit to the data (with model parameters and formal 1σ errors provided in Table 1 - although we caution that such errors do not necessarily reflect the complex shape of χ^2 space in such fits) with the corresponding spectral de-convolution shown in Figure 2. In addition to the model parameters, we extract the unabsorbed 0.3-8 keV integrated flux for the DISKBB and CUTOFFPL components using the pseudo-model CFLUX and provide the unabsorbed luminosities and errors in Table 1. We note that removing the DISKBB component and re-fitting the data with only TBABS*CUTOFFPL (with Γ and E_{cutoff} still fixed to those from the fit to the covariance spectrum), leads to a increase in $\Delta\chi^2$ of >3000 for 2 additional d.o.f, confirming that a soft component is statistically required in addition to the cutoff power-law revealed by the covariance.

As the spectral deconvolution differs from that presented in Brightman et al. (2018), we repeat the line significance test they describe, assuming the model is correct and testing for the chance occurrence of a similar or higher $\Delta\chi^2$ from adding the GABS component at any energy. In this model, the $\Delta\chi^2$ from adding the line is -45.14; across 100,000 simulated spectra, only 5 reached this value. Restricting our statistical analysis to only those observations of M51 ULX-8 in which the line was searched for in Brightman et al (2018), we correct the false alarm rate for the additional 8 observations where the line has not been detected (although as Brightman et al. 2018 point out, this may well be expected, as such lines vary and in most cases the data quality cannot rule out the presence of the CRSF). Our final, global false alarm rate is $< 4 \times 10^{-4}$ indicating a significance in excess of 3σ .

We allow the previously fixed CRSF parameters (energy and line-width) to vary and re-fit the time-averaged data. The resulting best-fit invokes a broader line ($\sigma \approx 1 \text{ keV}$) with an improvement of

$\Delta\chi^2 \approx 5$ for 2 d.o.f. Clearly, this is not a statistically significant improvement, yet without a clear requirement to keep the CRSF parameters fixed, we cannot rule out this solution (and indeed, when fitting the covariance spectrum with a broad line instead of a narrow one, neither the fit quality nor model parameters change significantly). Whilst such line parameters might be more in keeping with expectation for an eCRSF ($\sigma/E > 0.1$ – Tsygankov et al. 2006), it is apparent from inspection of the residuals to the best-fit that there is significant scatter around the line energy (see Figure 2) and some narrow structure around the previously reported CRSF line centroid. Whilst it is possible that CRSFs in such sources may have complex shapes (e.g. Fürst et al. 2015) – perhaps formed of both a broad and narrow component reflecting the dipole and higher-order, multipole fields, density and velocity gradients – we note that it is highly probable that the broad-line solution is being influenced by the curvature in the continuum. With forthcoming data extending the energy coverage for this source, we will be better able to address this issue. Due to the obvious issues and uncertainty in this spectral fit we do not repeat the significance test of Brightman et al. (2018) in this case.

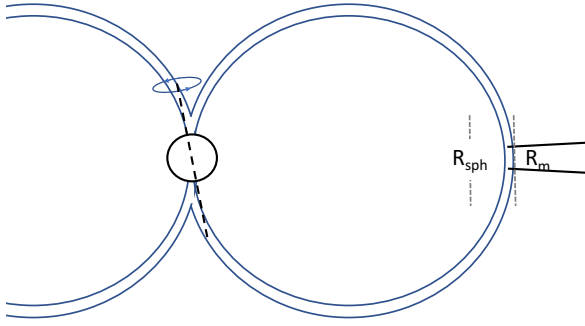
As our bandpass does not extend to the high energies where a hard excess above a Wien tail has been reported for a number of ULXs (e.g. Bachetti et al. 2013; Mukherjee et al. 2015; Walton et al. 2015), we cannot currently determine whether such an excess is present in this source. However, conceivably there could be an additional high energy component whose lower energy emission could extend into our bandpass and impact upon the parameter values we have obtained. To test for this, we introduce a further CUTOFFPL component with parameters based on the fits which isolate the pulsed component in NGC 7793 P13 (Walton et al. 2017), i.e. $\Gamma = 0.17$, $E_{\text{cutoff}} = 4.7 \text{ keV}$ and free normalisation. We find that, in the case of both of the fits described above, the parameters for the soft component (which will prove crucial in the following analysis) remain unchanged within 3σ .

3 TESTING THE DIPOLE FIELD STRENGTH

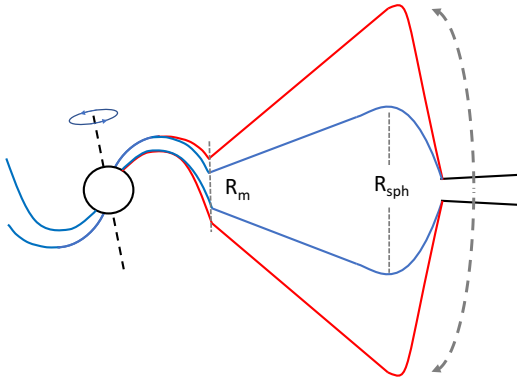
The spectral fits described above, guided by the covariance, have allowed us to obtain a clearer picture of the true spectral deconvolution for M51 ULX-8. Importantly we now have parameters that can be used to test the picture that the source harbours a strong (10^{15} G) dipole field. This needs to be tested in two distinct cases: where the flow beyond r_M is sub-critical or super-critical.

3.1 A sub-critical disc

Depending on mass accretion rate and dipole field strength, it is possible that an accretion disc which would otherwise greatly exceed the Eddington limit onto the neutron star can remain sub-critical (i.e. locally below the Eddington limit). The condition for this to occur is $r_M > r_{\text{sph}}$, where r_{sph} is the spherisation radius, the point at which the Eddington limit is reached in the disc (see Shakura & Sunyaev 1973 and Figure 3). Under such a condition, the disc remains geometrically thin and sub-critical down to r_M within which the material falls through an accretion curtain onto the neutron star via a shock-heated column (where the decrease in electron scattering cross section can allow for highly super-Eddington rates of infall, e.g. Mushtukov et al. 2015). Based on the spectral deconvolution, we would expect the hard, variable component to be from the accretion column whilst the soft component would correspond to the combined emission from the thin disc extending down



(a) a sub-critical disc geometry



(b) a super-critical disc geometry

Figure 3. A 2D schematic representation of the two models under consideration in the paper. In the top plot we show the *sub-critical* disc geometry where the thin disc truncates at R_M and forms a closed magnetosphere with an optical depth in this accretion ‘curtain’ determined in part by the magnetic field strength of the neutron star. In the bottom plot we show our favoured model for M51 ULX-8. At large radii the disc is geometrically thin (black lines) but as the Eddington luminosity is reached locally, the disc inflates until radiation pressure supports the flow at R_{sph} (blue lines). Within this radius, mass is lost via winds (red lines). Within R_M , material is confined to flow along field lines down to the surface of the neutron star where the CRSF is presumably imprinted (and potentially a $\sim 10^{15}$ G multipole field could be present). Precession of the inflow and outflow (perhaps as a consequence of Lense-Thirring torques, e.g. Middleton et al. 2018) could lead to a changing view of the inner regions as they are partially occulted and produce a correlated variable component at higher energies.

to r_M and accretion curtain (with the latter two having similar spectra when the curtain is optically thick: Mushtukov et al. 2017).

Should the above scenario be the correct physical description for M51 ULX-8, we require the accretion curtain to be optically *thin* such that the CRSF is not suppressed due to repeat scatterings. Mushtukov et al. (2017) determine the scattering conditions in the accretion curtain by considering the dynamics of the gas flowing from r_M , paying particular note to the geometry of the accretion column (which is affected by the dipole field strength; Mushtukov et al. 2015). The resulting condition for the accretion curtain material to be optically *thick* to electron scattering is $L_{39} \gtrsim B_{12}^{1/4}$ (where L_{39} is the accretion luminosity in units of 10^{39} erg s $^{-1}$ and B_{12} is the dipole field strength in units of 10^{12} G). Mushtukov et

al. (2017) determine that the actual optical depth of the curtain is a function of the distance along the path of the free-falling material and so reversing the above inequality provides only a *lower limit* on the field strength required for the entire curtain to be optically thin such that the CRSF is guaranteed to be detected. Given the time-averaged X-ray luminosity of the source in this observation ($\approx 5 \times 10^{39}$ erg s $^{-1}$), we would require field strengths in excess of 6×10^{14} G. It is plausible that a dipole field strength of $\sim 10^{15}$ G would allow the CRSF to be detected and lead to a somewhat (perhaps only partially) optically thin curtain which would then not leave a substantial imprint on the spectrum due to Comptonisation (although we speculate there should be intrinsic cyclotron emission from the sub-relativistic plasma spiralling along the field lines).

In addition to not suppressing the CRSF, the small number of scatterings of photons from the accretion column will also not significantly diminish any variability from this component (be it intrinsic to the column itself or as a consequence of precession of the dipole: Lipunov & Shakura 1980; Mushtukov et al. 2017). If we were to assume that the correlated variability we see is indeed from the column, then the lack of variability from the soft X-ray component would be consistent with a geometrically thin disc extending down to r_M , as the variability from such flows is typically low amplitude and only appears on relatively long timescales dictated by the local viscous frequency (e.g. Lyubarskii 1999; Ingram 2016).

As we will show, there are several issues with this picture for M51 ULX-8. The most obvious is that the soft X-ray component – which, as we have discussed, might be associated with a thin disc – has an unabsorbed luminosity at least 8 times the Eddington limit (even for a limiting neutron star mass of $2 M_\odot$: Demorest et al. 2010). In the absence of geometrical beaming (which would invoke a super-critical flow) or some otherwise unknown physical process, this is irreconcilable with a geometrically thin disc.

Should the spectrum be de-convolved for other ULXs, it is plausible that the soft X-ray component may have sub-Eddington luminosities for a neutron star primary (typically $< 2 \times 10^{38}$ erg s $^{-1}$). Importantly, should a CRSF also be observed, the accretion curtain must be optically thin which may then genuinely allow the soft emission to be identified with a geometrically thin, sub-critical disc. The tests we describe below – using the parameters of M51 ULX-8 as an example – take a simple parameter of the spectral model (namely the DISKBB normalisation) and can be used to determine whether a sub-critical disc is plausible in any given ULX where a neutron star is thought to be present, given the above conditions.

The position of r_M is commonly related to the surface dipole field strength and luminosity (e.g. Lamb et al. 1973; Cui 1997; Fürst et al. 2018) by:

$$r_M = 2.7 \times 10^8 B_{12}^{4/7} L_{37}^{-2/7} \quad [\text{cm}] \quad (1)$$

which assumes a canonical neutron star ($M_{NS} = 1.4 M_\odot$, $R_{NS} = 10$ km), where L_{37} is the (bolometric) accretion luminosity in units of 10^{37} erg s $^{-1}$ (assumed to be a good tracer of the mass accretion rate, with a radiative efficiency $\eta \approx 0.21$). The normalisation of the DISKBB component, N_{dbb} , is related to the corrected position of the disc inner edge (see Kubota et al. 1998) by:

$$r_{in} = \xi f_{col}^2 D_{10} \sqrt{\frac{N_{dbb}}{\cos(\theta)}} \quad [\text{km}] \quad (2)$$

where ξ is a correction factor of order unity (determined by Kubota

et al. 1998 to be ≈ 0.41), f_{col} is the colour temperature correction factor due to scattering/absorption in the disc atmosphere, D_{10} is the distance to the source in units of 10 kpc (in this case $D = 8.58$ Mpc — McQuinn et al. 2016) and θ is the angle of the disc to the line-of-sight. Combining the above equations (as $r_{\text{in}} = r_{\text{M}}$ in this sub-critical picture) allows L_{37} to be estimated for a range in θ and B_{12} .

We plot the results in Figure 4 (left-hand plot) for a representative value of $f_{\text{col}} = 1.7$ and using M51 ULX-8 as an example, with the approximate 1σ range in N_{dbb} from our spectral modelling, of 0.1 to 1.22, found by allowing the CRSF parameters to be fixed or free respectively (see Table 1).

In Figure 4 (right-hand plot), we also plot the predicted luminosity as a function of dipole field strength at the limit of the sub-critical disc model – the point where $r_{\text{M}} = r_{\text{sph}}$. We use the approximation, $r_{\text{sph}} \approx \dot{m}_0 r_{\text{isco}}$ (Shakura & Sunyaev 1973), where \dot{m}_0 is the mass transfer rate through the outer disc in units of the Eddington mass accretion rate at r_{isco} (the ISCO radius which we assume to be at $6\text{GM}/c^2$). As the disc is still (just) sub-critical in this picture, we assume that $L \propto \dot{m}_0$ (rather than in a super-critical disc where $L \approx L_{\text{Edd}}[1 + \ln(\dot{m}_0)]$ - Shakura & Sunyaev 1973) such that:

$$\dot{m}_0 = \frac{\dot{m}}{\dot{m}_{\text{Edd}}} = \frac{0.08L_{37}}{0.21L_{\text{Edd},37}} \approx 0.03L_{37}m_{\text{NS}}^{-1} \quad (3)$$

where m_{NS} is the neutron star mass in M_{\odot} which we take to be 1.4, 0.08 is the radiative efficiency at the ISCO (which underpins the formula for r_{sph} although noting that, in reality the radiative efficiency at the ISCO is probably closer to 0.06 for neutron star systems - Sunyaev & Shakura 1986). Combined with equation (1), we then obtain the general formula $L_{37} \approx 1300B_{12}^{4/9}$ for $r_{\text{M}} = r_{\text{sph}}$.

As can be seen from inspection of Figure 4 (right-hand plot), in order to maintain a sub-critical disc with a dipole field of 10^{15} G implies luminosities *not* in excess of $\approx 10^{41}$ erg s^{-1} . Whilst this is consistent with observations of M51 ULX-8, it is several orders of magnitude *below* that which would be inferred from our use of the DISKBB parameters for the same dipole field strength (Figure 4, left-hand plot). Although it is possible to hide much of the luminosity should the source be (almost exactly) edge-on, this is both highly unlikely and, in the case of M51 ULX-8, no eclipses have been reported over several observations (three of which are in excess of a day in duration - Brightman et al. 2018). In keeping with our initial expectation based on the inferred luminosity, we have found that the model for sub-critical accretion onto a neutron star with a dipole field strength of 10^{15} G is indeed invalid in the case of M51 ULX-8.

We note that Figure 4 would appear to suggest that lower dipole field strengths ($< 10^{12}$ G) *are* consistent with producing both the observed total luminosity and still be consistent with the above requirement to remain sub-critical (with the notable exception of the disc luminosity). However, a key requirement is that the accretion curtain be optically thin, which must be the case for M51 ULX-8 as the CRSF is observable; for a time-averaged luminosity of 5×10^{39} erg s^{-1} this is not possible for dipole field strengths below $\approx 6 \times 10^{14}$ G (Mushtukov et al. 2017).

As a further test of the validity of a geometrically thin disc in the spectrum of ULXs, we can consider whether it can avoid being radiation pressure dominated at r_{M} (noting that in the case of M51 ULX-8 we know that this cannot be the case given the luminosity is well in excess of the Eddington value for even a very

massive neutron star). The disc is expected to become radiation pressure dominated when (Padmanabhan 2001; Frank et al. 2002; Andersson et al. 2005):

$$r \lesssim 880\alpha^{2/21}\dot{m}_0^{16/21}\left(\frac{m_{\text{NS}}}{1.4}\right)^{1/3} \text{ [km]} \quad (4)$$

where α is the viscosity coefficient of Shakura & Sunyaev (1973), we have assumed that the opacity is dominated by electron scattering and have made the explicit assumption that this radius in the disc is much greater than that of the neutron star (see Andersson et al. 2005). Substituting for (3) and equating to (2) then leads to the condition that the disc is *not* radiation pressure dominated when:

$$N_{\text{dbb}} \gtrsim \frac{1.8 \times 10^4}{f_{\text{col}}^4 D_{10}^2} \alpha^{4/21} L_{37}^{32/21} m_{\text{NS}}^{-6/7} \cos(\theta) \quad (5)$$

Assuming $\alpha = 0.1$, $f_{\text{col}} = 1.7$ and $L_{37} \approx 500$, we find that, to obtain the range of normalisations from our fits, would imply that the disc could only avoid being radiation dominated for $\theta \gtrsim 86^\circ$ which, as we have argued previously, is highly unlikely.

3.2 A super-critical disc

We have strong evidence that, in the case of M51 ULX-8, a sub-critical disc cannot be accommodated and we must instead explore the case for a super-critical flow, i.e. $r_{\text{M}} < r_{\text{sph}}$ for a range in dipole field strengths. The key difference compared to the previous physical scenario is that, from r_{sph} down to r_{M} , the disc is now geometrically thick, with advection and mass loss via winds stabilising the accretion flow. Whilst the super-Eddington luminosity in the sub-critical case had to rely on a magnetic pressure supported accretion column and suppression of the electron scattering cross section in the presence of a strong magnetic field, here we have both a luminosity from a radiatively supported disc ($L \approx L_{\text{Edd}}[1 + \ln(\dot{m}_0)]$) and collimation of emission from within r_{sph} (which leads to a breakdown in the assumption of isotropy and results in geometrical beaming, e.g. King 2009; Middleton & King 2016). In the case of a sub-critical flow, the soft X-ray component can be associated with a thin disc (providing it meets the criteria discussed in this paper), whereas in the super-critical model, the soft X-ray component is assumed to be associated with emission from the spherisation radius where the disc is instead geometrically thick (see Figure 3). Such a geometry and the relevant temperatures in the spectra are presented in Poutanen et al. (2007); although this model was developed assuming a black hole primary, to first order we would not expect the presence of a neutron star primary to make a substantial difference to the soft X-ray emission – in the absence of direct irradiation by the neutron star, r_{sph} is independent of compact object type. Conversely - and deviating somewhat from the black hole model of Poutanen et al. (2007), the harder X-ray emission must be associated with some combination of the inner disc, accretion curtain and column (see for instance the simulations of Takahashi et al. 2018; Abarca et al. 2018).

Based on the formulae of Poutanen et al. (2007), the temperature of the soft component found from our spectral modelling implies $\dot{m}_0 \approx 20$ (for $f_{\text{col}} = 1.7$). In order to establish whether this is compatible with a 10^{15} G dipole field, we determine the critical accretion rate at which $r_{\text{M}} = r_{\text{sph}}$. In units of the Eddington rate this is $\dot{m}_0 \approx 28B_{12}^{4/9}$ (or in commonly used units of 10^{17} g s^{-1} as $\dot{m}_{17} \approx 700B_{12}^{4/9}$ where we have assumed the radiative efficiency at the ISCO is ≈ 0.08 - although see Sunyaev & Shakura 1986).

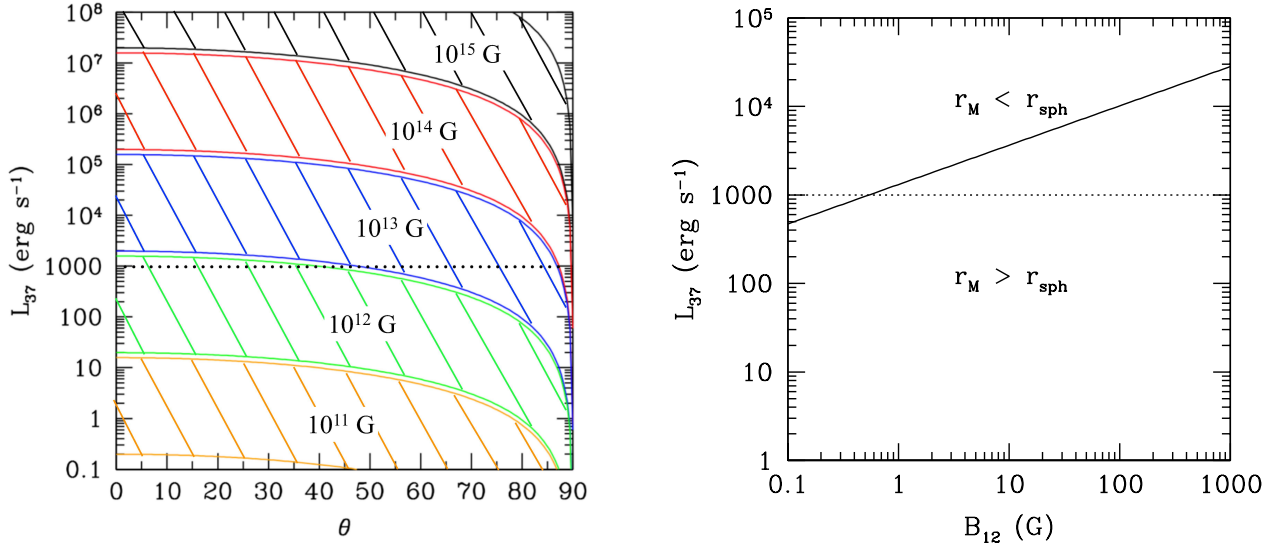


Figure 4. An example of the tests that can be applied to ULXs considered to harbour neutron stars where the soft component can be associated with a geometrically thin disc (e.g. when a CRSF is present such that the accretion curtain is optically thin). Left: the implied luminosity of M51 ULX-8 (in units of $10^{37} \text{ erg s}^{-1}$) versus inclination, from the combination of equations (1) and (2) (i.e. a model which assumes a disc where the Eddington limit is not reached locally) where $r_M = r_{\text{in}}$ and the DISKBB normalisation is taken from Table 1. The range of values for each dipole field strength results from the putative maximum range in N_{dbb} (assuming either case presented in Table 1) whilst the horizontal dotted line refers to the approximate observational limit on the luminosity from this source of $1 \times 10^{40} \text{ erg s}^{-1}$. Right: the limiting luminosity for the sub-critical model (once again in units of $10^{37} \text{ erg s}^{-1}$) versus dipole field strength (in units of 10^{12} G) which occurs when $r_M = r_{\text{sph}}$. From the left-hand plot, it is clear that the sub-critical model – based on the parameters for M51 ULX-8 – becomes invalid at field strengths in excess of $\sim 10^{13} \text{ G}$ as the inferred luminosity from the DISKBB normalisation would place the source into the super-critical regime in the right-hand plot.

From this, we determine that, for a 10^{15} G dipole field, $r_M = r_{\text{sph}}$ for $\dot{m}_0 \approx 600$, far above that implied by associating the soft component with emission from r_{sph} . As $\dot{m}_0 \approx 20$ with $B = 10^{15} \text{ G}$ would result in $r_M > r_{\text{sph}}$, we appear to be unable to construct a working model, be it sub- or super-critical, for M51 ULX-8 where the dipole field strength is so high.

Our spectral analysis and the restrictions described above, allow us to investigate whether a dipole field, similar in strength to those typically found in Galactic HMXBs (e.g. Fürst et al. 2014; Tendulkar et al. 2014; Yamamoto et al. 2014; Bellm et al. 2014) and potentially other ULPs at $\lesssim 10^{13} \text{ G}$ (e.g. King & Lasota 2016; King, Lasota & Kluzniak 2017; Christodoulou et al. 2016; Fürst et al. 2016), could account for the spectrum, luminosity and still allow for the observation of a CRSF. Using the previous formula, we determine that, for $\dot{m}_0 \approx 20$, we expect an upper limit on the dipole field strength of $\sim 10^{12} \text{ G}$ and the flow to be super-critical (with $r_{\text{sph}} \approx 120R_g$). As $r_M < r_{\text{sph}}$ in this case, the luminosity of the source results from the combination of the super-critical flow (minus that lost in an outflow), that from the accretion column (assuming $B > 10^9 \text{ G}$) and geometrical beaming. Whilst, in the sub-critical case such low field strengths would imply the accretion curtain is optically thick (Mushtukov et al. 2017), geometrical beaming of the emission by a factor of only a few allows the ac-

cretion curtain to start to become optically thin (see earlier discussion), thereby allowing us to detect the CRSF (when the view to the inner regions is not totally obscured by the thick disc and winds).

4 DISCUSSION & CONCLUSION

The degeneracy often inherent in time-averaged spectral fitting can be broken through time-resolved approaches, as we have demonstrated in the case of M51 ULX-8. Interpreting the $\approx 4.5 \text{ keV}$ line feature as a pCRSF implies either a dipole field of $\sim 10^{15} \text{ G}$ or a higher-order field of this strength closer to the neutron star surface (and falling off more rapidly with distance). As pointed out in Brightman et al. (2018), the width of the CRSF can indicate the responsible species, with electron CRSFs being typically broader ($\sigma/E_{\text{cyc}} \sim 0.1$; Tsygankov et al. 2006) than their proton counterparts ($\sigma/E_{\text{cyc}} < 0.1$; Ibrahim et al. 2002). Our analysis indicates that a broad component to the line cannot yet be ruled out although this may be a consequence of the limited energy coverage, and narrow structure is almost certainly still present (Figure 2).

Irrespective of the true shape of the line (and contributions from either the proton or electron populations), our use of the covariance has allowed us to effectively rule out a 10^{15} G dipole field in this source; in such a scenario, the luminosity is inconsistent with

the sub-critical interpretation and the accretion rate required to be super-critical is at odds with the spectrum. However, we stress that we do not rule out a $\sim 10^{15}$ G multipole field in this source.

We determine the likely upper bound for the dipole field strength to be $\sim 10^{12}$ G (consistent with the field strengths estimated from the spin-up rates seen in ULPs: e.g. King & Lasota 2016; Christodoulou et al. 2016; Fürst et al. 2016; King, Lasota & Kluzniak 2017; Carpano et al. 2018) and find that only a super-critical flow is able to reproduce the luminosity, spectrum and optically thin accretion curtain (the latter allowing us to observe the CRSF). In such a flow, the disc has a large scale-height from r_{sph} down to r_{M} and precession of this flow could potentially result in the repeated changes in flux seen in the hard spectral component from the inner-most regions (e.g. Dauser, Middleton & Wilms 2017); such a geometry is presented in Figure 3.

Should a multipole field (assumed to be $\sim 10^{15}$ G) be present in addition to the $< 10^{12}$ G dipole, a requirement of our model is that it should not dominate over the latter at the magnetospheric radius. This in turn requires that the field fall off as R^{-n} where $n \gtrsim 3 [\log(R_{\text{NS}}/R_{\text{M}})-1]/\log(R_{\text{NS}}/R_{\text{M}})$. In the case of our inferred super-critical disc with $\dot{m}_0 = 20$, this implies $n \gtrsim 5$ (at the limit of $r_{\text{M}} = r_{\text{sph}}$). Although this would appear to preclude the presence of a quadrupole field, we note that we have assumed the formulae relating to super-critical discs (in determining the accretion rate and location of r_{sph}) are free of uncertainties. Although unlikely to be the case, should they be accurate, we still cannot rule out an even higher order multipole field (e.g. a hexapole or octopole; Pétri 2015) leading to the reported CRSF.

A corollary of associating a more classical super-critical accretion flow to M51 ULX-8 is that we expect to detect line-of-sight atomic features in absorption (the mass-loaded, radiatively driven wind) and isotropic emission lines (perhaps due to shock heating between the wind and secondary star) as seen in other ULXs (Middleton et al. 2014, 2015b; Pinto et al. 2016, 2017; Walton et al. 2016a) and most recently in a ULP (Kosec et al. 2018). Detection of such atomic features in the spectrum of M51 ULX-8 in future (perhaps with the advent of χ RISM or Athena) would provide further confirmation regarding the nature of the inflow in this source. Whilst the CRSF in the spectrum of M51 ULX-8 is the clearest example of such a signal found to-date in a ULX, discovering more CRSFs directly or indirectly (e.g. Walton et al. 2018c) should allow the approaches we have outlined in this paper to be applied to other sources suspected of harbouring neutron stars (assuming the continuum can be deconvolved) and the nature of the accretion flow to be firmly established.

5 ACKNOWLEDGEMENTS

The authors thank the anonymous referee. MJM and DJW appreciate support from Ernest Rutherford STFC fellowships.

REFERENCES

- Abarca D., Kluzniak W., Sądowski A., 2018, MNRAS, 479, 3936
 Andersson N., Glampedakis K., Haskell B., Watts A. L., 2005, MNRAS, 361, 1153
 Arnaud K. A., 1996, ASPC, 101, 17
 Bachetti M., et al., 2013, ApJ, 778, 163
 Bachetti M., et al., 2014, Natur, 514, 202
 Basko M. M., Sunyaev R. A., 1976, MNRAS, 175, 395
 Bellm E. C., et al., 2014, ApJ, 792, 108
 Brightman M., et al., 2018, NatAs, 2, 312
 Carpano S., Haberl F., Maitra C., Vasilopoulos G., 2018, MNRAS, 476, L45
 Cui W., 1997, ApJ, 482, L163
 Christodoulou D. M., Kazanas D., Laycock S. G. T., 2016, arXiv, arXiv:1606.07096
 Dauser T., Middleton M., Wilms J., 2017, MNRAS, 466, 2236
 Demorest P. B., Pennucci T., Ransom S. M., Roberts M. S. E., Hessels J. W. T., 2010, Natur, 467, 1081
 Dickey J. M., Lockman F. J., 1990, ARA&A, 28, 215
 Farrell S. A., Webb N. A., Barret D., Godet O., Rodrigues J. M., 2009, Natur, 460, 73
 Frank J., King A., Raine D. J., 2002, apa.book, 398
 Fürst F., et al., 2014, ApJ, 780, 133
 Fürst F., et al., 2015, ApJ, 806, L24
 Fürst F., et al., 2016, ApJ, 831, L14
 Fürst F., et al., 2017, A&A, 606, A89
 Herold H., 1979, PhRvD, 19, 2868
 Ibrahim A. I., Safi-Harb S., Swank J. H., Parke W., Zane S., Turolla R., 2002, ApJ, 574, L51
 Ingram A. R., 2016, AN, 337, 385
 Israel G. L., et al., 2017, Sci, 355, 817
 Israel G. L., et al., 2017, MNRAS, 466, L48
 Jiang Y.-F., Stone J. M., Davis S. W., 2014, ApJ, 796, 106
 Kaaret P., Feng H., Roberts T. P., 2017, ARA&A, 55, 303
 King A. R., 2009, MNRAS, 393, L41
 King A., Lasota J.-P., 2016, MNRAS, 458, L10
 King A., Lasota J.-P., Kluzniak W., 2017, MNRAS, 468, L59
 Kosec P., Pinto C., Walton D. J., Fabian A. C., Bachetti M., Fürst F., Grefenstette B. W., 2018, arXiv, arXiv:1803.02367
 Kubota A., Tanaka Y., Makishima K., Ueda Y., Dotani T., Inoue H., Yamaoka K., 1998, PASJ, 50, 667
 Lamb F. K., Pethick C. J., Pines D., 1973, ApJ, 184, 271
 Lipunov V. M., Shakura N. I., 1980, SvAL, 6, 28
 Liu Q. Z., Mirabel I. F., 2005, A&A, 429, 1125
 Lyubarskii Y. E., 1997, MNRAS, 292, 679
 McQuinn K. B. W., Skillman E. D., Dolphin A. E., Berg D., Kennicutt R., 2016, ApJ, 826, 21
 Middleton M. J., Walton D. J., Roberts T. P., Heil L., 2014, MNRAS, 438, L51
 Middleton M. J., Heil L., Pintore F., Walton D. J., Roberts T. P., 2015, MNRAS, 447, 3243
 Middleton M. J., Walton D. J., Fabian A., Roberts T. P., Heil L., Pinto C., Anderson G., Sutton A., 2015, MNRAS, 454, 3134
 Middleton M. J., King A., 2016, MNRAS, 462, L71
 Middleton M. J., King A., 2017, MNRAS, 470, L69
 Middleton M. J., et al., 2018, MNRAS, 475, 154
 Mukherjee E. S., et al., 2015, ApJ, 808, 64
 Mushtukov A. A., Suleimanov V. F., Tsygankov S. S., Poutanen J., 2015, MNRAS, 454, 2539
 Mushtukov A. A., Suleimanov V. F., Tsygankov S. S., Ingram A., 2017, MNRAS, 467, 1202
 Mushtukov A. A., Ingram A., Middleton M., Nagirner D. I., van der Klis M., 2019, MNRAS, 484, 687
 Ohsuga K., Mineshige S., Mori M., Kato Y., 2009, PASJ, 61, L7
 Paczynski B., 1992, AcA, 42, 145
 Padmanabhan T., 2001, tass.book, 594
 Pasham D. R., Strohmayer T. E., 2013, ApJ, 774, L16
 Pétri J., 2015, MNRAS, 450, 714
 Pinto C., Middleton M. J., Fabian A. C., 2016, Natur, 533, 64
 Pinto C., et al., 2017, MNRAS, 468, 2865
 Pintore F., Zampieri L., Stella L., Wolter A., Mereghetti S., Israel G. L., 2017, ApJ, 836, 113
 Poutanen J., Lipunova G., Fabrika S., Butkevich A. G., Abolmasov P., 2007, MNRAS, 377, 1187
 Sądowski A., Narayan R., McKinney J. C., Tchekhovskoy A., 2014, MNRAS, 439, 503
 Shakura N. I., Sunyaev R. A., 1973, A&A, 24, 337
 Syunyaev R. A., Shakura N. I., 1986, SvAL, 12, 117
 Takahashi H. R., Mineshige S., Ohsuga K., 2018, ApJ, 853, 45

- Tendulkar S. P., et al., 2014, ApJ, 795, 154
Terashima Y., Inoue H., Wilson A. S., 2006, ApJ, 645, 264
Thompson C., Duncan R. C., 1995, MNRAS, 275, 255
Tsygankov S. S., Lutovinov A. A., Churazov E. M., Sunyaev R. A., 2006,
MNRAS, 371, 19
Uttley P., Cackett E. M., Fabian A. C., Kara E., Wilkins D. R., 2014,
A&ARv, 22, 72
Vaughan B. A., Nowak M. A., 1997, ApJ, 474, L43
Walton D. J., et al., 2015, ApJ, 806, 65
Walton D. J., et al., 2016, ApJ, 826, L26
Walton D. J., et al., 2016, ApJ, 827, L13
Walton D. J., et al., 2018, MNRAS, 473, 4360
Walton D. J., et al., 2018, ApJ, 856, 128
Walton D. J., et al., 2018, ApJ, 857, L3
Wilkinson T., Uttley P., 2009, MNRAS, 397, 666
Wilms J., Allen A., McCray R., 2000, ApJ, 542, 914
Yamamoto T., Mihara T., Sugizaki M., Nakajima M., Makishima K., Sasano
M., 2014, PASJ, 66, 59